

A review of machine learning applications for the proton MR spectroscopy workflow

Citation for published version (APA):

van de Sande, D. M. J., Merkofer, J. P., Amirrajab, S., Veta, M., van Sloun, R. J. G., Versluis, M. J., Jansen, J. F. A., van den Brink, J. S., & Breeuwer, M. (2023). A review of machine learning applications for the proton MR spectroscopy workflow. *Magnetic Resonance in Medicine*, 90(4), 1253-1270. <https://doi.org/10.1002/mrm.29793>

Document license:
CC BY-NC

DOI:
[10.1002/mrm.29793](https://doi.org/10.1002/mrm.29793)

Document status and date:
Published: 01/10/2023

Document Version:
Publisher's PDF, also known as Version of Record (includes final page, issue and volume numbers)

Please check the document version of this publication:

- A submitted manuscript is the version of the article upon submission and before peer-review. There can be important differences between the submitted version and the official published version of record. People interested in the research are advised to contact the author for the final version of the publication, or visit the DOI to the publisher's website.
- The final author version and the galley proof are versions of the publication after peer review.
- The final published version features the final layout of the paper including the volume, issue and page numbers.

[Link to publication](#)

General rights

Copyright and moral rights for the publications made accessible in the public portal are retained by the authors and/or other copyright owners and it is a condition of accessing publications that users recognise and abide by the legal requirements associated with these rights.

- Users may download and print one copy of any publication from the public portal for the purpose of private study or research.
- You may not further distribute the material or use it for any profit-making activity or commercial gain
- You may freely distribute the URL identifying the publication in the public portal.

If the publication is distributed under the terms of Article 25fa of the Dutch Copyright Act, indicated by the "Taverne" license above, please follow below link for the End User Agreement:

www.tue.nl/taverne

Take down policy










If you believe that this document breaches copyright please contact us at:

openaccess@tue.nl

providing details and we will investigate your claim.

REVIEW

A review of machine learning applications for the proton MR spectroscopy workflow

Dennis M. J. van de Sande¹  | Julian P. Merkofer²  | Sina Amirrajab¹  |
 Mitko Veta¹  | Ruud J. G. van Sloun^{2,3}  | Maarten J. Versluis⁴  |
 Jacobus F. A. Jansen^{2,5,6}  | Johan S. van den Brink⁴  | Marcel Breeuwer^{1,2,4} 

¹Department of Biomedical Engineering, Eindhoven University of Technology, Eindhoven, The Netherlands

²Department of Electrical Engineering, Eindhoven University of Technology, Eindhoven, The Netherlands

³Philips Research, Philips Research, Eindhoven, The Netherlands

⁴MR R&D - Clinical Science, Philips Healthcare, Best, The Netherlands

⁵Department of Radiology and Nuclear Medicine, Maastricht University Medical Center, Maastricht, The Netherlands

⁶School for Mental Health and Neuroscience, Maastricht University, Maastricht The Netherlands

Correspondence

Dennis M. J. van de Sande, Eindhoven University of Technology, PO Box 513, 5600 MB Eindhoven, The Netherlands.
 Email: d.m.j.v.d.sande@tue.nl

Funding information

This work was funded through ITEA4 as part of the Spectralligence project (EUREKA AI Call 2020), project number, Grant/Award Number: 20209

Abstract

This literature review presents a comprehensive overview of machine learning (ML) applications in proton MR spectroscopy (MRS). As the use of ML techniques in MRS continues to grow, this review aims to provide the MRS community with a structured overview of the state-of-the-art methods. Specifically, we examine and summarize studies published between 2017 and 2023 from major journals in the MR field. We categorize these studies based on a typical MRS workflow, including data acquisition, processing, analysis, and artificial data generation. Our review reveals that ML in MRS is still in its early stages, with a primary focus on processing and analysis techniques, and less attention given to data acquisition. We also found that many studies use similar model architectures, with little comparison to alternative architectures. Additionally, the generation of artificial data is a crucial topic, with no consistent method for its generation. Furthermore, many studies demonstrate that artificial data suffers from generalization issues when tested on in vivo data. We also conclude that risks related to ML models should be addressed, particularly for clinical applications. Therefore, output uncertainty measures and model biases are critical to investigate. Nonetheless, the rapid development of ML in MRS and the promising results from the reviewed studies justify further research in this field.

KEYWORDS

deep learning, machine learning, MR spectroscopic imaging, MR spectroscopy

1 | INTRODUCTION

MR spectroscopy (MRS) and MR spectroscopic imaging (MRSI) are noninvasive methods for investigating the

chemical and structural properties of molecules in vivo. These techniques are widely used for measuring human metabolism, particularly in the areas of neural diseases, tumor detection, and monitoring.¹⁻³ While MRS and MRSI

Dennis M. J. van de Sande and Julian P. Merkofer contributed equally to this work.

This is an open access article under the terms of the [Creative Commons Attribution-NonCommercial](https://creativecommons.org/licenses/by-nc/4.0/) License, which permits use, distribution and reproduction in any medium, provided the original work is properly cited and is not used for commercial purposes.

© 2023 The Authors. *Magnetic Resonance in Medicine* published by Wiley Periodicals LLC on behalf of International Society for Magnetic Resonance in Medicine.

have the potential to be highly valuable in clinical practice, they pose several challenges such as low signal-to-noise ratio (SNR), overlapping metabolite signals, experimental artifacts, and long acquisition times. To effectively analyze spectroscopy data, various considerations such as pulse sequence selection,⁴ B₀ shimming,⁵ as well as preprocessing and analysis methods^{6,7} must be taken into account. Due to the complexity of these considerations, MRS and MRSI can be challenging techniques for nonexperts to implement and oversee, hindering clinical adoption.³

The ability to learn model-agnostic features from data has made machine learning (ML) methods very popular in many disciplines over the last decade. In MRI the use of ML techniques, for example, has increasingly found a wide range of applications ranging from image reconstruction⁸⁻¹⁰ and quality improvement¹¹ to image analysis¹² and clinical diagnostics.¹³⁻¹⁶ This trend has started to increase in MRS and MRSI as well, with various ML methods being proposed to address some of the associated challenges. In the work of Chen et al.¹⁷ a sparse collection of such deep learning (DL)-based approaches is summarized. The work covers nine application examples in the domains of spectral reconstruction and denoising of proton MRS as well as chemical shift prediction and automated peak-picking for proton and other NMR spectroscopy. Another review by Rajeev et al.¹⁸ focuses on the clinical diagnosis of brain tumors from MR spectra using DL methods. The study condenses 20 data-driven approaches designed to improve the MRS workflow and consequently improve tumor diagnosis. However, an exhaustive collection of recent ML applications in MRS is still missing. Furthermore, these previous reviews do not show where the discussed ML studies fit into the MRS workflow, which inhibits better insight into the application domain. Moreover, with continuously emerging techniques in ML,¹⁹⁻²¹ the urgency for a thorough documentation of ML developments in MRS has grown persistently.

In this review we aim to bridge the gap between specific knowledge of the MRS workflow, from acquisition to clinical applications, and the technicalities of ML methods. Comprehensive and assessable summaries of recent ML studies are provided, based on their organization within common workflows of proton MRS. We discuss and summarize architectures, input and output schemes, training strategies, and the intended application for a selection of studies.

1.1 | Literature search

The literature search is conducted based on the systematic process outlined in Figure 1. To ensure a comprehensive overview, we focus on state-of-the-art ML studies of the last

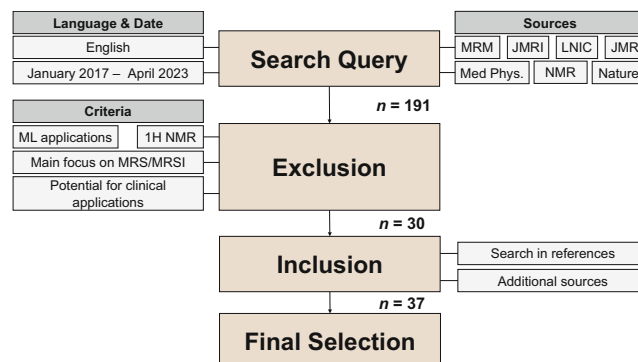


FIGURE 1 An outline of the systematic literature search. At start, the language and time period are set before a filter is applied for the selected sources. The Scopus search query results in a selection of publications which are manually checked on the exclusion criteria. After including additional sources, the final selection is obtained. The amount of papers after each step is indicated with n . The sources are Magnetic Resonance in Medicine (MRM), Journal of Magnetic Resonance Imaging (JMIR), Lecture Notes in Computer Science (LNIC) (including subseries Lecture Notes in Artificial Intelligence and Lecture Notes in Bioinformatics), Journal of Magnetic Resonance (JMR), Medical Physics (Med. Phys.), NMR in Biomedicine (NMR), and Nature.

7 years, as they hold the most relevance for current developments within the field. Using Elsevier's Scopus database the search is narrowed to studies published between and including January 2017 and April 2023 in major journals in the field of MR. By determining a specific query to search in title, keywords, and abstract for specific keywords related to MRS, MRSI, ML, DL, and neural networks (NNs) the search is further limited to 191 studies. The literature is excluded if it primarily focuses on other modalities than MRS and MRSI or do not mention ML applications. The final selection is obtained after investigating the references of the found literature and a final search using other search engines. Additional literature from other sources is added if their content fits within the scope. Table 1 provides an overview of the final 37 papers, covered in this review.

1.2 | MRS workflow

This review is structured following a common MRS and MRSI workflow.^{7,59} This workflow is applicable for clinical and research purposes and is divided into three main parts: data acquisition, processing, and analysis.

Data acquisition includes all the necessary steps for acquiring raw MRS or MRSI data, such as pulse sequence design, voxel placement, and B₀ shimming. The processing step involves techniques that reduce the dimensionality of the data, remove spectral imperfections, or improve

TABLE 1 Overview of all summarized and discussed studies with information about year, workflow category, training data type, model type, input, and output.

Study	Year	Category	Training data type	Model Type	Input	Output
Bolan et al. ²²	2020	Volume selection	In vivo	U-Net	T2w-FLAIR	Segmentation mask
Becker et al. ²³	2022	Shimming	Phantom	Ensemble	Four-dimensional spectra	Shim values
Becker et al. ²⁴	2022	Shimming	Phantom	LSTM	Spectrum + Shim offset	Shim values
Nassirour et al. ²⁵	2018	Reconstruction	In vivo	Multiple single-layer neural networks (NNs)	Undersampled k-space	k-Space values
Lee et al. ²⁶	2020	Reconstruction	In vivo + Artificial	U-Net	FID/Spectrum	FID/Spectrum
Luo et al. ²⁷	2020	Reconstruction	Artificial	HRNet	NUS L-COSY Spectrum	L-COSY Spectrum
Iqbal et al. ²⁸	2021	Reconstruction and quantification	Artificial	U-Net	NUS L-COSY Spectrum	L-COSY Spectrum
Motyka et al. ²⁹	2021	Reconstruction	In vivo	Shallow-graph CNN	Encoding step + FID point	k-Space points
Chan et al. ³⁰	2022	Reconstruction	In vivo	Multiple single-layer NNs	Undersampled k-Space	k-Space values
Lei et al. ³¹	2021	Spectral denoising	In vivo + Phantom	Autoencoder	Low NSA spectrum	High NSA spectrum
Iqbal et al. ³²	2019	Super-resolution MRSI	In vivo + Artificial	U-Net	LRSI image	HRSI image
Dong et al. ³³	2021	Super-resolution MRSI	In vivo	U-Net	LRSI Image	HRSI image
Tapper et al. ³⁴	2021	Frequency and phase correction	Artificial	MLP	Spectrum	Frequency/phase values
Ma et al. ³⁵	2022	Frequency and phase correction	Artificial	CNN	Spectrum	Frequency/phase values
Shamaei et al. ³⁶	2023	Frequency and phase correction	Artificial	Autoencoder	FID	FID (Corrected)
Kyathanahally et al. ³⁷	2018	Ghosting artifact removal	Artificial	MLP, CNN, Autoencoder	Spectrum/spectrogram	Ghost class (2)/spectrogram
Lee and Kim ³⁸	2019	General artifact removal	Artificial	CNN	Spectrum	Spectrum (Metabolites Only)
Pedrosa de Barros et al. ³⁹	2017	Quality assurance	In vivo	Random forest	FID + Spectral features	Quality class (2)
Gurbani et al. ⁴⁰	2018	Quality assurance	In vivo	CNN	Spectrum	Quality class (3)
Kyathanahally et al. ⁴¹	2018	Quality assurance	In vivo	SVM, LDA, RUSBoost	Spectral Features	Quality class (3)
Jang et al. ⁴²	2021	Quality assurance	Artificial	GAN	Spectrum	Quality class (2)
Hernández-Villegas et al. ⁴³	2022	Quality assurance	In vivo	NNMF	Spectrum	Quality class (3)
Das et al. ⁴⁴	2017	Quantification	In vivo + Artificial	Random forest	Spectrum	Metabolite concentrations

(Continues)

TABLE 1 (Continued)

Study	Year	Category	Training data type	Model Type	Input	Output
Hatami et al. ⁴⁵	2018	Quantification	Artificial	CNN	Spectrum	Metabolite concentrations
Gurbani et al. ⁴⁶	2019	Quantification	In vivo	Autoencoder	Spectrum	Spectrum
Lee and Kim ⁴⁷	2020	Quantification and uncertainty measurement	Artificial + Phantom	CNN	Spectrum	Spectrum (metabolite only)
Shamaei et al. ⁴⁸	2021	Quantification	Artificial	CNN	FID	Metabolite concentrations
Rizzo et al. ⁴⁹	2023	Quantification	Artificial	CNN, Ensemble	Spectrum/spectrogram	Metabolite concentrations
Schmid et al. ⁵⁰	2023	Quantification	Artificial	CNN, LSTM	Spectrum	Peak class (3)/Peak widths
Shamaei et al. ⁵¹	2023	Quantification	In vivo + Artificial	Autoencoder	FID	FID
Lee and Kim ⁵²	2022	Uncertainty measurement	Artificial	CNN	Spectrum	Spectrum
Rizzo et al. ⁵³	2022	Uncertainty measurement	Artificial	CNN	Spectrogram	Metabolite concentrations
Zarinabad et al. ⁵⁴	2017	Classification	In vivo	Ensemble	Spectrum/Metabolite Concentrations	Tumor class (3)
Zarinabad et al. ⁵⁵	2018	Classification	In vivo	SVM, LDA, Random Forrest	Metabolite Concentration features	Tumor class (3)
Dikaos ⁵⁶	2021	Classification	In vivo + Artificial	SVM, MLP, CNN	Spectrum	Tumor class (2)
Zhao et al. ⁵⁷	2022	Classification	In vivo	SVM, LDA, k-Means, Naive Bayes, NN	Metabolite concentration features	Tumor class (3)
Olliverre et al. ⁵⁸	2018	ML-based artificial data generation	In vivo	GAN	Noise vector	Spectrum

the visual appearance of the spectra. Some examples include signal averaging, eddy current correction, residual water/lipid removal, motion correction, apodization, and zero-filling. The analysis step involves using the processed data to evaluate its quality, quantify it with uncertainty, or classify it by specific characteristics such as disease. ML can be applied at each step of this workflow to perform or improve specific tasks. Additionally, some ML applications may require the use of artificial data for training, because there is a lack of large open databases. Since ML methods are highly dependent on the training data, artificial data generation is added as a workflow category. Figure 2 provides a schematic overview of the workflow, highlighting the use of ML at each step.

This review does not contain any introduction to ML methodology. For a comprehensive overview of ML, DL, and general artificial intelligence techniques we refer the reader to the alternative sources.⁶⁰⁻⁶² Schematic examples of some DL model types that are seen in Table 1, are shown in Figure 3. Additionally, we refer to alternative sources for principles and explanations of MRS concepts.^{59,63}

The structure of this review is as follows: in Section 2, relevant ML studies on data acquisition in the context of MRS and MRSI are summarized and discussed. In Sections 3 and 4 the same is done for processing and analysis respectively. Section 5 briefly discusses artificial data generation and in Section 6 an overall conclusion and outlook on the use of ML in MRS and MRSI is provided.

2 | DATA ACQUISITION

During data acquisition, scan-configuration parameters need to be optimized to get the desired and optimal data

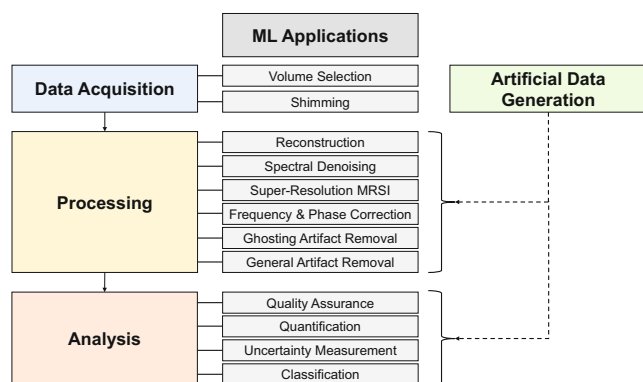


FIGURE 2 Schematic overview of the overall MR spectroscopy and MR spectroscopic imaging workflow with corresponding machine learning (ML) applications. The dashed arrows indicate a possibility to include artificial data into the development of some ML applications.

output. In this section some ML-based data acquisition methods are summarized and discussed.

2.1 | Volume selection

Voxel placement in single voxel spectroscopy is critical to limit partial volume effects, especially for the analysis of brain tumors. Bolan et al.²² propose an algorithm for automated voxel placement. They use a dataset of 60 low-grade glioma patients containing T2w fluid-attenuated inversion recovery images and corresponding MRS voxels manually placed by an expert spectroscopist. Lesion masks are retrospectively annotated by an experienced neuro-oncologist to have a gold-standard for training. The first step in their method involves tumor segmentation using a pre-trained convolutional neural network (CNN) model that is fine-tuned with their own dataset. The obtained segmentation volumes are used to maximize an objective function that describes the placement of a cuboid voxel in terms of position, size and rotation angle. This function captures two main considerations: voxel size and lesion fraction. Evaluation is done by comparing the lesion fraction, the volume of intersection between the annotated lesion and the MRS voxel, and the total voxel size between manually and automatically placed voxels. The authors found that the proposed automatic placement method has a higher lesion fraction compared to manually placed voxels. Moreover, their method demonstrates more consistent placement with lower SDs for lesion fraction, volume of intersection, and voxel size.

2.2 | Shimming

Performing B_0 shimming is important to obtain useful and high-quality MRS data.⁵ To accelerate and automate the shimming process, Becker et al.²³ propose a DL-based method for shimming. The used dataset contains raw ^1H -FID signals with shim offsets, in which only linear shims in orthogonal X , Y , and Z directions are considered. The DL method aims to predict shim values for the X , Y , and Z directions based on the one dimensional (1D) spectra of the linear shim offsets. They use an ensemble model architecture consisting of heterogeneous weak learners that are combined by either averaging, a fully connected layer, or a multilayer perceptron (MLP). Results show that both a single weak learner and the ensemble model with a MLP are able to predict shim values that improve spectral quality. These models are also used in combination with the downhill simplex method,⁶⁴ which is well-established for automatic shimming. They found that using their models, as stand-alone or in combination

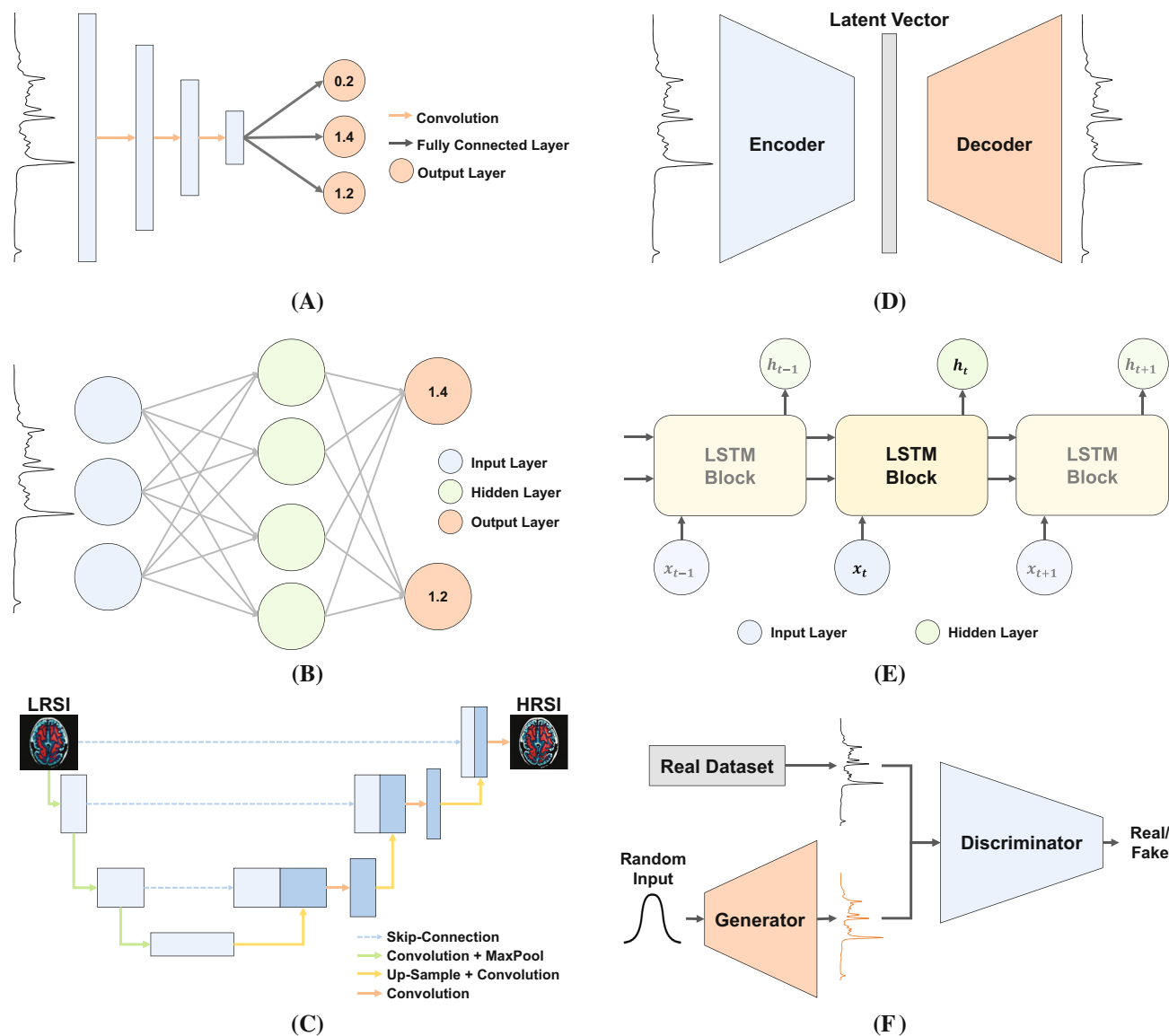


FIGURE 3 Overview of the most commonly used model types that are discussed in this review. In (A) a convolutional neural network architecture is visualized which takes a spectrum as input and outputs scalar values (i.e., metabolite concentrations). In (B) a multilayer perceptron is visualized with an arbitrary number of nodes. In (C) a U-Net model is visualized which performs super-resolution with a low-resolution spectroscopic imaging (low-resolution spectroscopic imaging (LRSI)) image as input and a high-resolution spectroscopic imaging image as output. In (D) a general autoencoder is visualized which aims to reconstruct the input spectrum in the output. In (E) a long short-term memory model is visualized which takes a (time) sequence input and uses feedback connections to calculate the next hidden layer. Variables x_t and h_t indicate the sequence value and hidden state at timestep t respectively. In (F) a generative adversarial network model is visualized that generates artificial spectra using a generator and includes a discriminator to determine whether a spectrum is real or fake. (A) Convolutional neural network (CNN) model type; (B) multilayer perceptron (MLP) model type; (C) U-Net model type; (D) Autoencoder model type; (E) Long short-term memory (LSTM) model type; (F) Generative adversarial network (GAN) model type.

with this simplex method, results in either a reduction in the number of acquisitions necessary or an improvement in spectral quality.

In a follow-up study, Becker et al.²⁴ extend their previous work by incorporating a higher-order shim (Z^2) and a different neural network (NN) architecture in their study. The proposed architecture uses a CNN combined with a long short-term memory (LSTM) block in order

to mimic a signal-based shimming technique where the previously obtained states, in the form of a 1D spectrum and a shim offset, are used in the process. The value of the shim offsets are dependent on the time step during training. First, a number of random steps are taken followed by a series of predictive steps for which the input shim offsets are the previously obtained values. The results show that using DL methods, with or without traditional

optimization algorithms, is more effective than using traditional optimization alone.

3 | PROCESSING

Raw MRS and MRSI measurements require a multitude of processing steps to obtain interpretable signals. Commonly recommended steps for MRS include coil combination, signal averaging, motion correction, eddy current correction, frequency and phase correction (FPC), and identification of spurious echoes.⁷ The following sections present and summarize ML studies that have shown to improve and replace such existing processing methods.

3.1 | Reconstruction

Efficient sampling and reconstruction techniques play an important role in accelerating MRS and MRSI methods. When the data is highly under-sampled, reconstructing spectra from truncated free induction decays (FIDs) creates truncation artifacts. Lee et al.²⁶ propose and compare three different reconstruction approaches with identically designed U-Net⁶⁵ architectures. The networks differ based on their inputs and outputs, which are either completely in the time domain, completely in the frequency domain, or mixed (FID in, spectrum out). In vivo 9.4T rat brain spectra are acquired to test the approaches as well as extract knowledge of the present SNR and linewidth values. Training data is obtained using a basis set simulation for 17 metabolites. The results show that the U-Net operating purely in the frequency domain has the best performance in terms of lowest normalized mean squared error and highest Pearson correlation coefficient (for the simulated data). The following observations are made with the simulated data: for 8 and 16 retained points (out of 1024) the U-Net recovers spectra with substantial truncation artifacts; for 32 and 64 retained points the approach manages to recover spectra with minor residuals; for 128 (and upwards) the truncation artifacts are well suppressed by the NN, enabling precise quantification.

In addition to 1D single voxel spectroscopy there are two-dimensional (2D) MRS techniques, such as the localized correlated spectroscopy (L-COSY) experiment.⁶⁶ Despite the long acquisition time for L-COSY, it can aid in distinguishing overlapping metabolites. Luo et al.²⁷ introduce an encoder-decoder network architecture for fast reconstruction of nonuniformly sampled L-COSY spectra by learning to predict fully sampled spectra from under-sampled input spectra. They propose to use simulated training data generated by the mode of virtual echo,⁶⁷ where the under-sampled spectra are obtained by

exponential and Poisson-gap sampling. This method is found to have fewer reconstruction artifacts and better peak preservation compared to other architectures such as CNN and U-Net. It is also further evaluated with multi-nuclei spectra and found to have similar reconstruction quality compared to an iterative soft thresholding approach⁶⁸ as well as sparse multidimensional iterative lineshape-enhanced reconstruction.⁶⁹

To accelerate L-COSY experiments, Iqbal et al.²⁸ propose a U-Net model to reconstruct fully sampled spectra using nonuniformly sampled spectra as an input. They test their approach on simulated L-COSY spectra with exponential sampling. Results suggest that the U-Net architecture not only produces good quality spectra for all tested acceleration factors (1.3×, 2×, and 4×), but also outperforms the compressed-sensing results of an $L1$ -norm minimization method for the higher acceleration factors.

Various acceleration techniques have been explored for MRSI,^{70,71} mainly through under-sampling of the k-space and reconstruction using compressed-sensing or parallel imaging techniques.⁷²⁻⁷⁴ Nassirpour et al.²⁵ propose to improve the conventional generalized autocalibrating partial parallel acquisition (GRAPPA) reconstruction⁷³ by estimating k-space weightings with multiple NNs to increase the overall applicability of high-resolution MRSI. They train two types of single-layer NNs to predict the missing data points; one for cross-neighbors and one for adjacent neighbors. During reconstruction, the two network types are deployed sequentially in such a way that first the cross-neighbor NNs fill in the missing k-space values and then the adjacent-neighbor NNs estimate the remaining points. Additionally, the authors propose variable density under-sampling schemes to achieve even higher acceleration factors and alter their ML framework by first using 2-voxel cross-neighbor and adjacent-neighbor NNs before using the previously mentioned 1-voxel neighbor NNs. Although in this work the networks are trained in a subject-specific manner, various strategies are investigated in Reference 30 to improve this approach with more samples. The results suggest the use of NNs for GRAPPA reconstruction reduces aliasing artifacts thereby positively impacting metabolite concentration maps and significantly boosting the performance compared to regular GRAPPA.

Furthermore, Motyka et al.²⁹ propose a k-space-based coil combination using geometric DL to reduce the amount of processing data immediately after the acquisition instead of reducing the data in the image domain. Their approach utilizes a shallow-graph NN⁷⁵ to learn the k-space representation of the MRSI data before the summation step of the coil combination. In vivo data are augmented for training and pairs consisting of input and desired output for each partition encoding step and each

FID point are created. Additionally, white Gaussian noise is added to the training samples to increase the robustness of the method. The proposed method is compared to the conventional image-based coil combination iMUSICAL.⁷⁶ For both approaches, the metabolite concentration maps and the Cramér-Rao lower bound percentage value (CRLBP%) are similar to the results of LCMoel.⁷⁷ The proposed method performs comparable to iMUSICAL when evaluated for different SNRs levels, slightly under-performing for high SNR domains.

3.2 | Spectral denoising

SVS acquisition time linearly depends on the number of signal averages which are obtained to enhance the SNR. Learning the mapping between low number of signal averages (NSA) spectra to high NSA spectra can effectively denoise and improve the SNR of the MRS signal.

Lei et al.³¹ propose an autoencoder model to denoise MRS spectra. For that purpose they acquire multiple phantom and in vivo spectra with a NSA of 192 and of 8, representing high and low SNR. The proposed network consists of an encoder-decoder architecture, taking the processed low NSA spectra as the input in the frequency domain and outputting high NSA spectra with reduced noise. To enlarge the data variability a patch-based input is used in combination with data augmentation. The network is optimized using the mean squared error of the output spectra and the ground truth (GT) high SNR spectra including a $L1$ -norm on the hidden feature vector to enforce sparsity. SNR estimates of the input and output spectra show an SNR improvement of 40% and 47% for phantom and in vivo data, respectively, showing potential to accelerate MRS acquisitions by acquiring low NSA spectra while maintaining spectral quality.

3.3 | Super-resolution MRSI

Long acquisition times and high field strengths are often necessary to obtain high-resolution spectroscopic imaging (HRSI) data. Advanced post-processing methods to increase the resolution for low-resolution spectroscopic imaging (LRSI) data can be beneficial for reaching the desired resolution. Iqbal et al.³² propose a supervised DL method for super-resolution of MRSI data. They propose a U-Net architecture to take a T1w image and corresponding LRSI image as inputs and produce a HRSI image as output. In total, three different U-Nets are trained for three different LRSI resolutions (16×16 , 24×24 , and 32×32). They use synthetic data, generated by a MRSI simulator, for training and testing. This generator produces T1w

images and a pair of LRSI and HRSI data. The synthetic data is used to evaluate the trained models based on the mean squared error of the HRSI reconstructions and the reconstruction of individual spectra at different resolutions. Additionally, the models are tested on downsampled in vivo HRSI data. During evaluation, different noise levels are tested and a comparison is performed with standard methods like zero-filling and bicubic interpolation. Results show that the DL method performs better than standard methods for all noise levels and can be used as a denoising or acceleration method.

In a follow-up study, Dong et al.³³ propose another super-resolution model which included in vivo MRI and MRSI data. A dataset of HRSI (64×64) data is acquired and down-sampled to obtain LRSI (16×16) data. In total, 320 metabolic maps from three different patients are used as GT. The DL method consists of a U-Net with four different input modalities: LRSI data, T1-weighted images, fluid-attenuated inversion recovery images and contrast-enhanced T1-weighted images. The decoding part of the network uses spatial attention modules which automatically calculate spatial weight maps to focus on important features in each input modality. The HRSI output is used to calculate the loss function, which consists of three different parts. The first part is a pixelwise mean squared error loss, calculated by comparing the output with the GT data. To account for inter-pixel correlations, a second term called the multiscale structural similarity index is added. The multiscale structural similarity index measures the similarity between two different images at multiple scales in terms of luminance, contrast and structure. Finally, a discriminator is added to calculate an adversarial loss and capture more complex features. This study investigates the contribution of all different loss terms and input modalities by training multiple models. Results show that including all aforementioned inputs and losses achieves the best performance, also out-performing standard bi-cubic interpolation.

3.4 | Frequency and phase correction

FPC is necessary to reduce the effects of scanner frequency drifts, subject motion, or other inconsistencies to ensure reliable quantification without line broadening or loss in SNR. This is especially crucial in J-difference edited MRS spectra which rely on accurately subtracting two aligned spectra.

Tapper et al.³⁴ propose an automated FPC framework consisting of two separate NNs. A simulated dataset is obtained using ideal excitation/refocusing pulses and shaped editing pulses. The simulation parameters are chosen to match the in vivo data (Big GABA repository⁷⁸)

as close as possible. Both corrections are implemented with two sequentially placed fully connected NNs, where the frequency shifts are estimated first, followed by an estimation of the phase offsets. Both models are trained individually taking the magnitude or real-only spectra, respectively, as the input to predict the frequency or phase offsets. Results for simulated test data show accurate predictions with a mean frequency offset error reported at 0.00 ± 0.03 Hz and a mean phase offset error of -0.11 ± 0.25 degrees. Evaluation with in vivo data shows similar performance to a model-based spectral registration method,⁷⁹ however, they indicate a substantial performance degradation compared to the simulated data.

Based on this work, Ma et al.³⁵ propose an alternative DL approach for FPC using CNN architectures. They use identical parameter configurations to simulate MEGA-point resolved spectroscopy (PRESS) data for training and validation. However, they create additional spectra with lower SNRs by adding Gaussian noise. The authors observe less subtraction artifacts with the CNN and show an overall better performance than the approach of Tapper et al.³⁴ For the simulated data the authors report a mean frequency offset error of 0.02 ± 0.02 Hz for the MLP and 0.01 ± 0.01 Hz for the CNN, and a mean phase offset error of 0.19 ± 0.17 degree for the MLP and 0.12 ± 0.09 degree for the CNN. For the in vivo scenarios, performance is measured based on the variance of the choline metabolite of the spectra subtraction. The CNN performs better in 66.67%, 60.61%, and 75.76% of the 33 datasets, when small, medium, and large offsets are added to the data, respectively.

Shamaei et al.³⁶ develop unsupervised methods for FPC including two different convolutional encoder-model decoder (CEMD) models in which the input spectra are used as targets during training. One model focuses on reference peak fitting of creatine and uses a convolutional encoder to construct a lower-dimensional latent representation of the input. The latent parameters are used as input for a Lorentzian lineshape model decoder. The second CEMD model uses the same encoder, but a spectral registration function is used as decoder. To account for unstable frequency components, both models are also trained for a limited frequency range (2.5–3.5 ppm). Training and validation is done on a simulated dataset with known frequency and phase offsets and evaluation is done on phantom data and in vivo data from the Big GABA repository. The proposed unsupervised methods are compared with commonly used FPC methods (spectral registration and creatine referencing, both on full and limited frequency ranges) and previous DL methods.^{34,35} In contrast to the non-DL FPC methods, the CEMD models perform equally well when trained and applied on a limited frequency range and their performance is less influenced by

the presence of nuisance peaks. Compared to the previous DL methods, the CEMD is able to train in an unsupervised fashion and requires only one network for both frequency and phase correction.

3.5 | Ghosting artifact removal

Ghosting artifacts, or so-called spurious echos, are usually caused by insufficient spoiling gradient power in combination with local susceptibility variations. These artifacts negatively influence the reliability of metabolite quantification as they may overlap with metabolite peaks.

Kyathanahally et al.³⁷ evaluate two networks based on fully connected NNs and CNNs for the detection as well as an autoencoder network with residual blocks for the removal of ghosting artifacts. Brain metabolite spectra are simulated for ideal PRESS characteristics, and ghosting artifacts with varying line-widths and amplitudes are added randomly. The fully connected NN is trained on 1D spectra as input and class probabilities as output. An alternative classification approach is implemented with a CNN, taking the real and imaginary part of a 2D spectrogram as input. The spectrograms are obtained by segmenting the time domain signals followed by a Fourier transform of each segment, creating 2D time–frequency spectrograms. To effectively remove the ghosting artifacts, an autoencoder network is implemented, taking the 2D corrupted spectrograms as input and outputting artifact-free spectrograms. The authors report a classification accuracy between 50% and 75% for the fully connected NN depending on the number of layers. In contrast, the CNN approach shows promising performance with a mean accuracy of 94% for smaller datasets and an accuracy of over 99% for larger training sets and subsequent in vivo evaluations. In addition, the autoencoder method is found to be effective in removing ghost artifacts from distorted spectra, with low root mean squared error reported for the difference between ground truth and restored spectra in simulated data. However, the restoration is found to be suboptimal for in vivo cases.

3.6 | General artifact removal

The previously discussed methods all focus on a specific processing step, yet NNs have the ability to learn more complex mappings from training data, enabling multiple artifact corrections at once. Lee and Kim³⁸ propose a CNN architecture taking spectra contaminated with artifacts as input and predicting noise-free, metabolite-only spectra. The NN is trained using simulated data with metabolite

phantom spectra as a basis set and knowledge of in vivo data for specific linewidth, SNR, and baseline ranges. Further, in vivo test data is obtained from five healthy volunteers with identical scanner settings used for the phantom spectra of the basis set. For both simulated and in vivo data, the CNN clearly manages to obtain spectra with removed noise, narrow linewidth, removed frequency and phase shifts, and without spectral baseline. The results show no visible residual signal and thus suggest good removal of artifacts only in the simulated scenario. Further, the reported mean absolute percent error of the quantification estimates and the GTs concentrations is $20.67\% \pm 16.71\%$. For the in vivo spectra the results of the proposed method coincide with estimates of LCMoel as well as commonly reported metabolite concentrations from the literature.

4 | ANALYSIS

The MRS analysis focuses on converting the (processed) signals into meaningful and reliable metabolite concentration estimates. The following subsections summarize recent ML applications for spectral quality assurance, metabolite quantification, uncertainty measurement, and classification.

4.1 | Quality assurance

MRS and MRSI methods are susceptible to various imperfections causing artifacts in the acquired spectra which in turn can create unreliable and inaccurate measurements. This limits the clinical use of MRS and causes a dependence on technical experts to inspect the spectral quality.

De Barros et al.³⁹ introduce an active learning method to improve labeling efficiency based on spectral quality by either accepting or rejecting spectra for further analysis. The method uses a dataset of over 28 000 in vivo spectra from brain tumor patients. Forty-seven features are extracted from the time-domain and frequency-domain magnitude spectra and are used as input for a random forest (RDF) classifier. Two expert spectroscopists manually label the spectra to provide GT for supervised training. The active learning strategy employs an uncertainty range defined as $[0.5 - \alpha, 0.5 + \alpha]$, where α controls the width. When the RDF classifier's output falls within this range, the uncertain data instance is added to the training set. This active learning method is evaluated iteratively, where in each iteration spectra from one patient are evaluated and uncertain examples are added to the training set. After retraining, the RDF classifier is validated on one patient (leave-one-out-cross-validation). Results show insignificant or minor differences in classification

performance between different values for α ($0.1 \leq \alpha \leq 0.5$), resulting in an efficient way of training a RDF classifier with fewer manual labeling.

Gurbani et al.⁴⁰ propose a CNN architecture to automatically classify the quality of a given spectrum and integrate it into a software pipeline enabling real-time filtering of echo-planar spectroscopic imaging data. In vivo spectra from patients with glioblastoma are collected after appropriate filtering. These spectra are then reviewed by MRS experts and classified as "Good," "Acceptable," or "Poor" quality to obtain GT labels for the NN. The CNN architecture takes the normalized real component of the spectrum as input and splits it into six specific regions, each with its own designated CNN. These CNNs are trained in parallel by passing their concatenated outputs through a MLP of which the output represents the probability to be classified as "Good." The overall model performs well in terms of detecting "Poor" quality spectra with an area under the curve of 0.951.

Kyathanahally et al.⁴¹ evaluate various ML approaches for fast quality classification of MR spectra. The authors perform training and testing on the multicenter studies INTERPRET⁸⁰ and eTUMOUR⁸¹ consisting of more than 1000 spectra, mostly already classified into good and bad quality. Furthermore, they create an intermediate class for "Poor" quality if one of the three experts thought the spectrum was acceptable, and they also create their own local expert ratings for some previously unlabeled data. The authors evaluate various classifiers based on support vector machines (SVMs), linear discriminant analysis (LDA), and random undersampling and boosting in combination with independent component analysis and principal component analysis (PCA) or sequential forward feature selection and bootstrap-aggregated decision trees as feature extraction or feature selection methods. Their final approach uses a high number of features as input and a random undersampling and boosting classifier that under-samples to combat the imbalanced training data, showing a comparable performance in rejecting unsuitable spectra to a human expert.

Hernández-Villegas et al.⁴³ propose a convex nonnegative matrix factorization for the same multicenter studies used in Reference 41 to distinguish between good and poor quality spectra. The method first iteratively factorizes observations into a source matrix (of data centroids) and a mixing matrix (containing combination weights). Then, two experts define quality measures based on correlation and Euclidean distance of the extracted sources of 10 repetitions as well as based on the coding coefficient of the mixing matrices. Thereby, spectral quality can be assessed and characterized in an unsupervised fashion. The obtained results indicate that the defined quality measures can identify sources containing artifacts and the approach

manages to distinguish between good- and poor-quality spectra.

Jang et al.⁴² train a generative adversarial network (GAN) to detect abnormalities in 3T human brain spectra. Normal and abnormal brain spectra are simulated, similarly to Lee and Kim.³⁸ Eight different classes of spectra are generated that are abnormal in SNR, linewidth, a single metabolite concentration, multiple metabolites concentrations (9), or all factors combined. Additionally, spectra that contain ghosting, residual water, or residual lipid artifacts are simulated with the help of phantom data. After training the GAN on normal spectra only, latent space mapping is performed. This mapping is done with a loss function containing a dissimilarity term that compares the generator output with the input spectra, and a discriminator term that uses feature matching from the second last layer of the discriminator. The classification between normal and abnormal spectra is performed with a 2D threshold using normalized mean squared error and the SD of the spectra. Results show over 80% accuracy for some abnormalities such as SNR and N-acetylaspartate concentration. Additionally, the GAN also detects ghosting, residual water, and residual lipid artifacts without using those spectra in the training phase. However, the model cannot accurately detect abnormalities in linewidth and low-concentrated metabolites with accuracies of around 50%.

4.2 | Quantification

Quantification aims at converting processed MRS spectra/-FIDs into specific metabolite concentration estimates. Traditionally, model-based methods employed for metabolite quantification include linear combination model fitting, peak fitting, and peak integration.^{82,83}

An early ML-based quantification approach is introduced by Das et al.⁴⁴ where they propose a RDF regression method. The proposed model is developed with different combinations of artificial spectra and in vivo spectra. The RDF consists of a set of binary trees with splits based on random subsets of the feature variables on which the forest is subsequently trained. The trees of the RDF are trained using piece-wise linear regression over the input spectrum outputting metabolite concentration estimates, followed by taking the weighted average of the predictions from each tree to obtain a single output estimate. Results show that the RDF technique has similar performance as LCModel and could therefore be used in combination with LCModel to assist with the quantification of noisy spectra and enable faster convergence.

Hatami et al.⁴⁵ propose a supervised CNN model for metabolite quantification which is able to cover 20 different metabolites and a macromolecule signal. The

CNN takes real and imaginary parts of the spectra as a two-channel input and outputs concentrations of all metabolites of interest. A training and test with GT concentrations are obtained by simulating spectra based on an MRS signal model. To evaluate the accuracy of the quantification model, the symmetric mean absolute percent error over the whole test set is calculated and compared with the performance of the model-based QUEST⁸⁴ method and the previously mentioned RDF regression algorithm from Das et al.⁴⁴ The proposed CNN outperforms the other methods with and without the addition of noise.

Shamaei et al.⁴⁸ investigate the use of a CNN which used a wavelet scattering transformation to extract features from the MRS signal. The extracted features are fed into a fully connected feed-forward NN to predict the relative amplitudes of the metabolite basis spectra, which can be used for absolute quantification. For training and evaluation, multiple datasets are simulated by using a signal-based model and uniform sampling of its parameters. Their model shows better performance, in terms of symmetric mean absolute percent error, compared to QUEST and similar performance as the model of Hatami et al.⁴⁵ Additionally, the wavelet scattering CNN shows robustness against metabolite phase changes and nuisance signals, such as macromolecules.

Gurbani et al.⁴⁶ use a CEMD for spectral fitting. This two-step unsupervised DL approach takes the real part of the spectrum as an input. During the first encoder-decoder step, a spectrum is mapped to a lower-dimensional space and a baseline is reconstructed using a wavelet reconstruction decoder. The resulting baseline is subtracted from the input spectrum and fed into the second encoder-decoder network, which is used to reconstruct the spectral lineshape, and therefore the fitting parameters for the metabolites of interest. Three metabolites are considered including choline, creatine, and N-acetylaspartate. The final CEMD model is also included in a pipeline for creating whole-brain metabolite maps for patients with glioblastoma and is compared with MIDAS.⁸⁵ Results show that both methods have similar fitting performance and the choline/N-acetylaspartate maps created by the CEMD have a Dice score of 0.72 when compared to MIDAS.

Lee and Kim⁴⁷ propose a CNN architecture to quantify metabolite concentrations. Their approach consists of a designated CNN per metabolite, taking the real part of a spectrum as input to estimate the corresponding metabolite spectrum. The actual quantification of the metabolites is then obtained by computing the areas of the known spectral regions relative to the methyl signal of total creatine (creatine (Cr) + phosphocreatine (PCr)) (tCr). The results for the proposed quantification approach show a

well-performing algorithm for the completely synthetic scenarios (i.e., mean absolute percent error of 1.92% and 2.56% for the methyl [~ 3.0 ppm] and methylene [~ 3.9 ppm] peaks for the reference metabolite tCr). For the simulated spectra using metabolite phantoms and in vivo baselines the mean absolute percent error is increased as depicted above and ranged from $14.79 \pm 11.12\%$ to $23.07 \pm 16.36\%$ over the major metabolites.

Similarly, Iqbal et al.²⁸ propose a method with a designated NN per metabolite implemented using U-Nets. Their approach takes the real, imaginary, and magnitude information of a fully sampled L-COSY spectrum as input and outputs the magnitude spectrum for each of the seventeen metabolites. The authors observe an increase in error for both degrading SNR and higher water signal amplitude. Nonetheless, the model shows accurate quantification of the metabolites, even for low concentrations.

Rizzo et al.⁴⁹ compare MRS quantification using various CNN models, input types, and learning methods. They use a simulated artifact-free dataset with GT concentrations to enable fair comparison with standard model fitting. Results indicate that 2D spectrogram inputs outperform 1D frequency domain inputs and that including a water reference peak improves performance. The best model is a heterogeneous ensemble combining 1D and 2D inputs while increasing dataset size and applying active learning strategies do not significantly improve performance. However, DL-based quantification still underperforms compared to standard model fitting and is highly biased toward training data when SNR is low.

Schmid et al.⁵⁰ propose a DL-based peak detection method as part of classical peak fitting. A simulated dataset, including various distortions, is used for training. Their CNN model with LSTM blocks outputs classes (baseline, narrow peak, or broad peak) and values for the peak widths. Input spectra are dynamically scaled to enhance local contrast and peak labels are acquired with an automatic labeling procedure. The outputs are used to fix the number of peaks and initialize the peak width values for a classical peak fitting algorithm. Evaluations on simulated and experimental data show high scores on picking accuracy, spectral reconstruction, and sparsity of the peak selection. Their method outperforms using manual peak picking in terms of mean absolute error, especially in crowded regions (i.e., 82% lower mean absolute error). The authors state that their method, although optimized for high-field proton spectroscopy, is adaptable to different domains.

Shamaei et al.⁵¹ implement a physics-informed DL method to quantify simulated spectra and in vivo spectra from the Big GABA repository.⁷⁸ They use a CEMD architecture with an encoder that outputs parameters for the signal-based model decoder. This decoder uses a

metabolite basis set and a numeric, parameterized, or regulated parameterized macromolecule signal contribution as prior knowledge. Their experiments include the investigation of different architectures for the encoder, the use of different macromolecule models, and different dataset sizes. Results show comparable performance to traditional quantification methods and the ability to use this DL approach for in vivo data, with best performances for shallow CNN encoders and minimum dataset sizes of 12 000 samples. Additionally, a numerical macromolecule signal is favorable above parameterized and regulated parameterized macromolecule models. Due to the unsupervised training approach and the significant reduction in computation time, this method could be used as a faster alternative to quantify large, in vivo MRS datasets.

4.3 | Uncertainty measurement

Uncertainty measurements of metabolite concentration estimates, such as the Cramér-Rao lower bound (CRLB) or the CRLBP% are crucial for assuring reliable results, yet for data-driven methods such measures are generally biased and alternative metrics are difficult to validate.

Lee and Kim⁴⁷ propose a CNN-based approach to quantify metabolite concentrations and simultaneously obtain an uncertainty estimate for the output spectra. The approach is developed with simulated rat brain spectra and is further evaluated using phantom data and in vivo rat brain spectra. The authors obtain a measurement uncertainty with respect to SNR, linewidth, and signal-to-background ratio (SBR) by constructing an uncertainty measurement database from the training data. The SNR and linewidth are estimated from the input spectrum, specifically from total N-acetylaspartate, while the SBR of each metabolite is measured from the predicted metabolite spectra. Then a three-dimensional (3D) space of the quantitative errors is computed and stored for each target metabolite as a function of the SNR, linewidth, and SBR. The estimated quantification uncertainty of the proposed method is highly correlated with the actual errors obtained in a purely simulated scenario (i.e., 0.81 ± 0.13 ; 0.88 ± 0.09 for 15 major metabolites). The correlation between predicted error and GT error for the simulated spectra using metabolite phantoms and in vivo baselines are slightly lower (i.e., 0.7 or higher [0.78 ± 0.05] and statistically significant for all 15 major metabolites).

In another work of Lee and Kim,⁵² they propose an alternative CNN architecture and training procedure to obtain both an estimate of metabolite concentrations and their uncertainties. Using Monte Carlo dropout⁸⁶ and a variance leveraging loss function based on the log-likelihood⁸⁷ both epistemic (model) and aleatoric

(data) uncertainty estimates are obtained for each metabolite concentration. The CNN is trained with simulated spectra, further tested with in vivo data, and shows comparable performance to model-based alternatives such as LCMoel.

The work of Rizzo et al.⁵³ investigates the reliability of DL-based quantification and compared it to common model fitting methods. For that purpose, they design a CNN taking spectrograms as input and outputting normalized metabolite concentration estimates. In a similar fashion to Lee et al.⁵² the authors use Monte Carlo dropout for epistemic (model) uncertainty and metrics based on bias and spread of the predicted concentration distribution for aleatoric (data) uncertainty information. The results indicate that the CNN's predictions tend toward the mean of the training data in cases with high uncertainty, indicating the model is biased. Meanwhile, model fitting methods show on average to be unbiased.

4.4 | Classification

Classification in MRS and MRSI data is important for clinical applications in terms of diagnosis and disease monitoring. Instead of using metabolite concentrations, ML methods can be trained to perform direct classification.

In a multiclass pediatric brain tumor classification problem, Zarinabad et al.⁵⁴ show that various ML methods can distinguish between three different tumor classes. An unbalanced dataset (in vivo, 1.5T) is used in combination with borderline synthetic minority oversampling technique (bSMOTE) (based on the synthetic minority oversampling technique algorithm⁸⁸) to increase classification performance. The trained classifiers consist of a RDF classifier with an adaptive number of trees and four different AdaBoostM1 algorithms using different weak learners: naive Bayes, support vector machine (SVM), NN, and LDA. Classification is done by either using the full spectra or the metabolite concentrations quantified by TARQUIN.⁸⁹ Oversampling the minority class with bSMOTE results in better classification performances of the trained classifiers, both for concentrations and spectral inputs. The best balanced accuracy rates are 0.93 and 0.90 for concentrations and spectral inputs respectively, with different combinations of classifiers and oversampling rates possible.

A similar classification problem is investigated in a subsequent study from Zarinabad et al.⁵⁵ However, the spectra are acquired on 3T scanners from four different hospitals. The tested classification algorithms are LDA, SVM, and RDF approaches and bSMOTE is used to account for the class imbalance. PCA is performed on the metabolite profiles to extract four principal components which are used as input for the classification algorithms.

The results show a maximum balanced accuracy of 0.86 when using SVM as a classification method, which compares favorably with a previous 1.5T multicenter study.⁹⁰

For the same multiclass tumor classification, Zhao et al.⁵⁷ propose to add metabolite selection. This study compares PCA and multiclass receiver operating characteristic as metabolite selection methods for training ML classifiers: LDA, *k*-nearest neighbors, naive Bayes, NN, and SVM. The classification with three tumor classes is done for both 1.5T and 3T single voxel spectroscopy data from multiple sites and oversampling for minority classes is done using the synthetic minority oversampling technique algorithm. Final classification accuracy is determined using *k*-fold and leave-one-out cross-validation. Metabolite selection using multiclass receiver operating characteristic shows a higher accuracy compared to PCA with the highest balanced classification accuracy of 85% for the 1.5T data with SVM and 75% for the 3T data with LDA. A more transparent and explainable tool for diagnosis is obtained by selection of metabolites for ML-based classification.

Dikaio⁵⁶ trains three different ML methods to differentiate metastasis from glioblastoma brain tumors. The models include SVM, MLP, and CNN. Different versions of the models with varying hyperparameters and/or layers are tested on four different datasets consisting of real GE spectra with additional noise, real Philips spectra with additional noise, synthetic GE spectra, and synthetic Philips spectra. A total of 12 models are trained using long echo time, short echo time, and concatenations of both versions of the spectra. Evaluation of the results, in terms of receiver operating characteristic-area under the curve and accuracy, shows the best performance for the 1D CNN when using synthetic data and the concatenated echo times (>90% accuracy).

5 | ARTIFICIAL DATA GENERATION

Accessing in vivo MRS/MRSI data is limited due to time-consuming acquisitions, nonstandardized methods,⁹¹ and privacy concerns. To overcome this limitation, artificial data generation is used for developing ML applications. All previously discussed studies, containing artificial data, use non-ML-based generation methods like data augmentation and model-based simulation. Data augmentation is a method that artificially increases the size and variety of the used dataset by applying transformations to real samples. On the other hand, model-based simulation involves sampling the parameters of a parametric model to generate MRS data, which is essentially an inverse use of signal-based fitting models. While the

concepts of artificial data generation are the same, the exact implementation varies a lot per study.

ML methods can also be applied for artificial data generation itself. The work of Olliverre et al.⁵⁸ focuses on generative models for creating MRS spectra. This study compares three different models (GAN, deep convolutional GAN (DCGAN), and pairwise mixture model⁹²) on their ability to generate MRS spectra for three classes: healthy, low-grade, and high-grade tissue. The models are trained on a dataset consisting of 137, 1.5T PRESS acquired in vivo spectra. The GAN model uses a generator and discriminator with fully connected layers and the DCGAN uses a deeper architecture, which generally requires more data. The DCGAN is therefore trained by using the full training dataset as batch size with the addition of batch normalization to deal with the relatively small dataset. All models are trained on all three tissue types separately and the quality of the artificially generated data is tested by training a RDF classifier. Results show that datasets generated by the GAN and pairwise mixture model are able to train a RDF classifier to the same level as using real MRS data. The DCGAN generated data has lower performance due to the small dataset size that underutilizes the potential of deep learning.

6 | CONCLUSION AND OUTLOOK

This review highlights recent ML studies within the field of proton MRS, focusing primarily on processing and analysis of MRS spectra and MRSI images with less attention on data acquisition. Although some studies have applied ML to volume selection for single voxel spectroscopy and shimming, other aspects of data acquisition (e.g., pulse sequence design, suppression techniques, and excitation area) have so far been disregarded. Due to the hardware-dependent nature of such applications, they are not only more difficult to integrate, but also to develop and test. Meanwhile, topics like quality assurance, quantification, and classification are more commonly addressed. Through the ability to simulate processed spectra or to rely on large databases for training data, such ML models are more straightforward to develop. In the future, more acquisition-oriented simulations could bridge this gap.

Recent ML studies focus on DL model types instead of classical ML methods like SVM, RDF, LDA, or PCA. Table 1 reveals that the most commonly used model type is a CNN. Additionally, most autoencoders, U-Nets, and ensemble model types also include convolutional layers. CNNs are widely adapted in computer vision and medical imaging^{93,94} with their benefits of weight sharing,

simultaneously extracting features and performing classification, and easy implementation into large-scale networks.⁹⁵ While recent studies from Rizzo et al.⁴⁹ and Shamaei et al.⁵¹ compare different model architectures, more comparison studies are still missing. Future work should focus on testing different and new model types like transformers that have shown potential in other medical imaging fields.⁹⁶ These types of studies can aid in finding the best practices for MRS and MRSI applications. As the field of ML rapidly evolves, it is important to keep up-to-date with new developments and investigate their role in MRS and other spectroscopy domains.

Section 5 mentions that many studies use different techniques to generate artificial data to develop their ML methods, making the comparability between different studies very challenging. Also, significant performance drops are observed when models are trained with artificial data and tested on in vivo data, showing difficulties in transferability from artificial data to in vivo data. This stems not only from lacking generalization capabilities of the ML methods, but also from the difficulty of accurately replicating in vivo data through simulation or synthesis. While metabolite signals are well understood using density matrix simulations, other signal contributions, like macromolecules, water/fat residuals, and other artifacts, remain challenging to simulate. Therefore, efforts that investigate and standardize (artificial) data generation, as well as augmentation techniques, are crucial for future research.

ML methods rely on their training data to learn meaningful tasks and are inherently biased towards this data. Without preventive or predictive measures there are no guarantees for the model's performance for inputs outside of this distribution.⁹⁷ Furthermore, the model's output might even collapse to the mean of its target distribution for mismatched inputs.⁹⁷ In a clinical setting, such behaviors need to be detected and removed. Reliable and broadly applicable uncertainty measures for ML prediction are therefore crucial for clinical applicability of ML in MRS. Additionally, deploying hybrid models (combined model-based and data-driven systems) can allow ML contributions to be leveraged by physics-informed models that behave unbiased and have guarantees on their estimates.⁹⁸

The clinical utility of ML applications in MRS and MRSI is one of the most important aspects of this research field. Attempts to decrease human-expert involvement, decrease acquisition time, and increase robustness and generalizability of existing MRS tools are therefore essential. ML methods should also be easy to interpret by clinicians to be useful in clinical workflows. While ML in MRS and MRSI is still in the early stages, the discussed studies show great potential for clinical adoption with plenty of future research possibilities.

ACKNOWLEDGMENTS

This work was (partially) funded by Spectralligence (EUREKA IA Call, ITEA4 project 20209).

CONFLICT OF INTEREST STATEMENT

The authors declare no potential conflict of interest.

ORCID

Dennis M. J. van de Sande  <https://orcid.org/0000-0001-6112-1437>

Julian P. Merkofer  <https://orcid.org/0000-0003-2924-5055>

Sina Amirrajab  <https://orcid.org/0000-0001-8226-7777>


Mitko Veta  <https://orcid.org/0000-0003-1711-3098>

Ruud J. G. van Sloun  <https://orcid.org/0000-0003-2845-0495>

Maarten J. Versluis  <https://orcid.org/0000-0003-3601-0377>

Jacobus F. A. Jansen  <https://orcid.org/0000-0002-5271-8060>

Johan S. van den Brink  <https://orcid.org/0000-0002-7058-4449>

Marcel Breeuwer  <https://orcid.org/0000-0003-1822-8970>

REFERENCES

- Buonocore MH, Maddock RJ. Magnetic resonance spectroscopy of the brain: a review of physical principles and technical methods. *Rev Neurosci*. 2015;26:609-632.
- Faghihi R, Zeinali-Rafsanjani B, Mosleh-Shirazi MA, et al. Magnetic resonance spectroscopy and its clinical applications: a review. *J Med Imaging Radiat Sci*. 2017;48:233-253.
- Wilson M, Andronesi O, Barker PB, et al. Methodological consensus on clinical proton MRS of the brain: review and recommendations. *Magn Reson Med*. 2019;82:527-550.
- Landheer K, Schulte RF, Treacy MS, Swanberg KM, Juchem C. Theoretical description of modern 1H in vivo magnetic resonance spectroscopic pulse sequences. *J Magn Reson Imaging*. 2020;51:1008-1029.
- Juchem C, Cudalbu C, Graaf RA, et al. B0 shimming for in vivo magnetic resonance spectroscopy: experts' consensus recommendations. *NMR Biomed*. 2021;34:e4350.
- Jansen JFA, Backes WH, Nicolay K, Kooi ME. 1H MR spectroscopy of the brain: absolute quantification of metabolites. *Radiology*. 2006;240:318-332.
- Near J, Harris AD, Juchem C, et al. Preprocessing, analysis and quantification in single-voxel magnetic resonance spectroscopy: experts' consensus recommendations. *NMR Biomed*. 2021;34:e4257.
- Knoll F, Hammernik K, Zhang C, et al. Deep-learning methods for parallel magnetic resonance imaging reconstruction: A survey of the current approaches, trends, and issues. *IEEE Signal Process Mag*. 2020;37:128-140.
- Montalt-Tordera J, Muthurangu V, Hauptmann A, Steeden JA. Machine learning in magnetic resonance imaging: image reconstruction. *Phys Med*. 2021;83:79-87.
- Arghya P, Yogesh R. A review and experimental evaluation of deep learning methods for MRI reconstruction. *J Mach Learn Biomed Imag*. 2022;1:1.
- Guangming Z, Bin J, Liz T, Yuan X, Greg Z, Max W. Applications of deep learning to neuro-imaging techniques. *Front Neurol*. 2019;10:869.
- Mohammed BA, Al-Ani MS. Review research of medical image analysis using deep learning. *UHD J Sci Technol*. 2020;4:75-90.
- Uddin LQ, Dajani DR, Voorhies W, Bednarz H, Kana RK. Progress and roadblocks in the search for brain-based biomarkers of autism and attention-deficit/hyperactivity disorder. *Transl Psychiatry*. 2017;7:e1218.
- Rashid B, Calhoun V. Towards a brain-based predictome of mental illness. *Hum Brain Mapp*. 2020;41:3468-3535.
- Pilmeyer J, Huijbers W, Lamerichs R, Jansen JF, Breeuwer M, Zinger S. Functional MRI in major depressive disorder: A review of findings, limitations, and future prospects. *J Neuroimaging*. 2022;32:582-595.
- Santana CP, de Carvalho EA, Rodrigues ID, Bastos GS, de Souza AD, de Brito LL. Rs-fMRI and machine learning for ASD diagnosis: A systematic review and meta-analysis. *Sci Rep*. 2022;12:6030.
- Chen D, Wang Z, Guo D, Orekhov V, Qu X. Review and Prospect: deep learning in nuclear magnetic resonance spectroscopy. *Chem A Eur J*. 2020;26:10391-10401.
- Rajeev SK, Pallikonda Rajasekaran M, Krishna Priya R, Al Bimani A. A review on magnetic resonance spectroscopy for clinical diagnosis of brain tumour using deep learning. Paper presented at: 2021 3rd International Conference on Advances in Computing, Communication Control and Networking (ICAC3N); 2021; Greater Noida, India:461-465.
- Wang X, Zhao Y, Pourpanah F. Recent advances in deep learning. *Int J Mach Learn Cybern*. 2020;11:747-750.
- Marcus G. The next decade in AI: four steps towards robust artificial intelligence. *arXiv:2002.06177*; 2020.
- Sarker IH. Deep learning: a comprehensive overview on techniques, taxonomy, applications and research directions. *SN Comput Sci*. 2021;2:420.
- Bolan PJ, Branzoli F, Di Stefano AL, et al. Automated acquisition planning for magnetic resonance spectroscopy in brain cancer. *Med Image Comput Comput Assist Interv*. 2020;12267:730-739. doi:10.1007/978-3-030-59728-3_71
- Becker M, Jouda M, Kolchinskaya A, Korvink JG. Deep regression with ensembles enables fast, first-order shimming in low-field NMR. *J Magn Reson*. 2022;336:107151.
- Becker M, Lehmkuhl S, Kesselheim S, Korvink JG, Jouda M. Acquisitions with random shim values enhance AI-driven NMR shimming. *J Magn Reson*. 2022;345:107323.
- Nassirpour S, Chang P, Henning A. MultiNet PyGRAPPA: multiple neural networks for reconstructing variable density GRAPPA (a 1H FID MRSI study). *Neuroimage*. 2018;183:336-345.
- Lee H, Lee HH, Kim H. Reconstruction of spectra from truncated free induction decays by deep learning in proton magnetic resonance spectroscopy. *Magn Reson Med*. 2020;84:559-568.
- Luo J, Zeng Q, Wu K, Lin Y. Fast reconstruction of non-uniform sampling multidimensional NMR spectroscopy via a deep neural network. *J Magn Reson*. 2020;317:106772.

28. Iqbal Z, Nguyen D, Thomas MA, Jiang S. Deep learning can accelerate and quantify simulated localized correlated spectroscopy. *Sci Rep*. 2021;11:8727.
29. Motyka S, Hingerl L, Strasser B, et al. k-Space-based coil combination via geometric deep learning for reconstruction of non-Cartesian MRSI data. *Magn Reson Med*. 2021;86:2353-2367.
30. Chan KL, Ziegs T, Henning A. Improved signal-to-noise performance of MultiNet GRAPPA 1H FID MRSI reconstruction with semi-synthetic calibration data. *Magn Reson Med*. 2022;88:1500-1515.
31. Yang L, Bing J, Tian L, Curran Walter J, Hui M, Xiaofeng Y. Deep learning-based denoising for magnetic resonance spectroscopy signals. Paper presented at: Medical Imaging 2021: Biomedical Applications in Molecular, Structural, and Functional Imaging, Online. California, USA; 2021:3.
32. Iqbal Z, Nguyen D, Hangel G, Motyka S, Bogner W, Jiang S. Super-resolution 1H magnetic resonance spectroscopic imaging utilizing deep learning. *Front Oncol*. 2019;9:1010.
33. Dong S, Hangel G, Bogner W, et al. High-resolution magnetic resonance spectroscopic imaging using a multi-encoder attention U-net with structural and adversarial loss. Paper presented at: 2021 43rd Annual International Conference of the IEEE Engineering in Medicine & Biology Society (EMBC), Online. Guadalajara, Mexico; 2021:2891-2895.
34. Tapper S, Mikkelsen M, Dewey BE, et al. Frequency and phase correction of J-difference edited MR spectra using deep learning. *Magn Reson Med*. 2021;85:1755-1765.
35. Ma DJ, le HAM, Ye Y, et al. MR spectroscopy frequency and phase correction using convolutional neural networks. *Magn Reson Med*. 2022;87:1700-1710.
36. Shamaei A, Starcukova J, Pavlova I, Starcuk Z Jr. Model-informed unsupervised deep learning approaches to frequency and phase correction of MRS signals. *Magn Reson Med*. 2023;89:1221-1236.
37. Kyathanahally SP, Döring A, Kreis R. Deep learning approaches for detection and removal of ghosting artifacts in MR spectroscopy: detection and removal of ghosting artifacts in MRS using deep learning. *Magn Reson Med*. 2018;80:851-863.
38. Lee HH, Kim H. Intact metabolite Spectrum mining by deep learning in proton magnetic resonance spectroscopy of the brain. *Magn Reson Med*. 2019;82:33-48.
39. Pedrosa de Barros N, McKinley R, Wiest R, Slotboom J. Improving Labeling efficiency in automatic quality control of MRSI data. *Magn Reson Med*. 2017;78:2399-2405.
40. Gurbani SS, Schreibmann E, Maudsley AA, et al. A convolutional neural network to filter Artifacts in spectroscopic MRI. *Magn Reson Med*. 2018;80:1765-1775.
41. Kyathanahally SP, Mocioiu V, Pedrosa de Barros N, et al. Quality of clinical brain tumor MR spectra judged by humans and machine learning tools. *Magn Reson Med*. 2018;79:2500-2510.
42. Jang J, Lee HH, Park JA, Kim H. Unsupervised anomaly detection using generative adversarial networks in 1H-MRS of the brain. *J Magn Reson*. 2021;325:106936.
43. Hernández-Villegas Y, Ortega-Martorell S, Arús C, Vellido A, Julià-Sapé M. Extraction of artefactual MRS patterns from a large database using non-negative matrix factorization. *NMR Biomed*. 2022;35:e4193.
44. Das D, Coello E, Schulte RF, Menze BH. Quantification of metabolites in magnetic resonance spectroscopic imaging using machine learning. In: Descoteaux M, Maier-Hein L, Franz A, Jannin P, Collins D, Duchesne S, eds. *Medical Image Computing and Computer Assisted Intervention - MICCAI 2017*. Lecture Notes in Computer Science. Springer; 2017:462-470.
45. Hatami N, Sdika M, Ratiney H. Magnetic resonance spectroscopy quantification using deep learning. In: Frangi A, Schnabel J, Davatzikos C, Alberola-López C, Fichtinger G, eds. *Medical Image Computing and Computer Assisted Intervention - MICCAI 2018*. Lecture Notes in Computer Science. Springer; 2018:467-475.
46. Gurbani SS, Sheriff S, Maudsley AA, Shim H, Cooper LAD. Incorporation of a spectral model in a convolutional neural network for accelerated spectral fitting. *Magn Reson Med*. 2019;81:3346-3357.
47. Lee HH, Kim H. Deep learning-based target metabolite isolation and big data-driven measurement uncertainty estimation in proton magnetic resonance spectroscopy of the brain. *Magn Reson Med*. 2020;84:1689-1706.
48. Shamaei A, Starčuková J, Starčuk Z Jr. A wavelet scattering convolutional network for magnetic resonance spectroscopy signal quantitation. Paper presented at: Proceedings of the 14th International Joint Conference on Biomedical Engineering Systems and Technologies, Online. Vienna, Austria; 2021:268-275.
49. Rizzo R, Dziadosz M, Kyathanahally SP, Shamaei A, Kreis R. Quantification of MR spectra by deep learning in an idealized setting: investigation of forms of input, network architectures, optimization by ensembles of networks, and training bias. *Magn Reson Med*. 2023;89:1707-1727.
50. Schmid N, Bruderer S, Paruzzo F, et al. Deconvolution of 1D NMR spectra: A deep learning-based approach. *J Magn Reson*. 2023;347:107357.
51. Shamaei A, Starcukova J, Starcuk Z Jr. Physics-informed deep learning approach to quantification of human brain metabolites from magnetic resonance spectroscopy data. *Comput Biol Med*. 2023;158:106837.
52. Lee HH, Kim H. Bayesian deep learning-based 1H-MRS of the brain: metabolite quantification with uncertainty estimation using Monte Carlo dropout. *Magn Reson Med*. 2022;88:38-52.
53. Rizzo R, Dziadosz M, Kyathanahally SP, Reyes M, Kreis R. Reliability of quantification estimates in MR spectroscopy: CNNs vs traditional model fitting. In: Wang L, Dou Q, Fletcher PT, Speidel S, Li S, eds. *Medical Image Computing and Computer Assisted Intervention - MICCAI 2022*. Springer; 2022:715-724.
54. Zarinabad N, Wilson M, Gill SK, Manias KA, Davies NP, Peet AC. Multiclass imbalance learning: improving classification of Pediatric brain Tumors from magnetic resonance spectroscopy: imbalanced learning for MRS tumor classification. *Magn Reson Med*. 2017;77:2114-2124.
55. Zarinabad N, Abernethy LJ, Avula S, et al. Application of pattern recognition techniques for classification of Pediatric brain Tumors by in vivo 3T 1H-MR spectroscopy – a multi-Center study. *Magn Reson Med*. 2018;79:2359-2366.
56. Nikolaos D. Deep learning magnetic resonance spectroscopy fingerprints of brain tumours using quantum mechanically synthesised data. *NMR Biomed*. 2021;34:e4479.
57. Zhao D, Grist JT, Rose HEL, et al. Metabolite selection for machine learning in childhood brain tumour classification. *NMR Biomed*. 2022;35:e4673.
58. Olliverre N, Yang G, Slabaugh G, Reyes-Aldasoro CC, Alonso E. Generating magnetic resonance spectroscopy imaging data of

- brain tumours from linear, non-linear and deep learning models. In: Gooya A, Goksel O, Oguz I, Burgos N, eds. *Simulation and Synthesis in Medical Imaging*. Lecture Notes in Computer Science. Springer; 2018:130-138.
59. Kreis R, Boer V, Choi I-Y, et al. Terminology and concepts for the characterization of in vivo MR spectroscopy methods and MR spectra: background and experts' consensus recommendations. *NMR Biomed*. 2021;34:e4347. doi:10.1002/nbm.4347
 60. LeCun Y, Bengio Y, Hinton G. Deep learning. *Nature*. 2015;521:436-444.
 61. Goodfellow I, Bengio Y, Courville A. *Deep Learning. Adaptive Computation and Machine Learning*. The MIT Press; 2016.
 62. Burkov A. *The Hundred-Page Machine Learning Book*. Andriy Burkov; 2019.
 63. De Graaf Robin A. *In Vivo NMR Spectroscopy: Principles and Techniques*. 3rd ed. John Wiley & Sons, Inc; 2019.
 64. Press WH. *Numerical Recipes: The Art of Scientific Computing*. 3rd ed. Cambridge University Press; 2007.
 65. Ronneberger O, Fischer P, Brox T. U-net: convolutional networks for biomedical image segmentation. *Medical Image Computing and Computer-Assisted Intervention – MICCAI 2015*. Lecture Notes in Computer Science. Springer; 2015:234-241.
 66. Thomas MA, Yue K, Binesh N, et al. Localized two-dimensional shift correlated MR spectroscopy of human brain. *Magn Reson Med*. 2001;46:58-67.
 67. Mayzel M, Kazimierczuk K, Orekhov VY. The causality principle in the reconstruction of sparse NMR spectra. *Chem Commun*. 2014;50:8947-8950.
 68. Hyberts SG, Milbradt AG, Wagner AB, Arthanari H, Wagner G. Application of iterative soft thresholding for fast reconstruction of NMR data non-uniformly sampled with multidimensional Poisson gap scheduling. *J Biomol NMR*. 2012;52:315-327.
 69. Ying J, Delaglio F, Torchia DA, Bax A. Sparse multidimensional iterative Lineshape-enhanced (SMILE) reconstruction of both non-uniformly sampled and conventional NMR data. *J Biomol NMR*. 2017;68:101-118.
 70. Vidya Shankar R, Chang JC, Hu HH, Kodibagkar VD. Fast data acquisition techniques in magnetic resonance spectroscopic imaging. *NMR Biomed*. 2019;32:e4046.
 71. Bogner W, Otazo R, Henning A. Accelerated MR spectroscopic imaging—a review of current and emerging techniques. *NMR Biomed*. 2021;34:e4314. doi:10.1002/nbm.4314
 72. Pruessmann KP, Weiger M, Scheidegger MB, Boesiger P. SENSE: sensitivity encoding for fast MRI. *Magn Reson Med*. 1999;42:952-962.
 73. Griswold MA, Jakob PM, Heidemann RM, et al. Generalized autocalibrating partially parallel acquisitions (GRAPPA). *Magn Reson Med*. 2002;47:1202-1210.
 74. Breuer FA, Martin B, Mueller MF, et al. Controlled aliasing in volumetric parallel imaging (2D CAIPIRINHA). *Magn Reson Med*. 2006;55:549-556.
 75. Zhou J, Cui G, Hu S, et al. Graph neural networks: A review of methods and applications. *AI Open*. 2020;1:57-81.
 76. Moser P, Bogner W, Hingerl L, et al. Non-Cartesian GRAPPA and coil combination using interleaved calibration data – application to concentric-ring MRSI of the human brain at 7T. *Magn Reson Med*. 2019;82:1587-1603.
 77. Provencher SW. Estimation of metabolite concentrations from Localized in vivo proton NMR spectra. *Magn Reson Med*. 1993;30:672-679.
 78. Mikkelsen M, Barker PB, Bhattacharyya PK, et al. Big GABA: edited MR spectroscopy at 24 research sites. *Neuroimage*. 2017;159:32-45.
 79. Near J, Edden R, Evans CJ, Paquin R, Harris A, Jezard P. Frequency and phase drift correction of magnetic resonance spectroscopy data by spectral registration in the time domain: MRS drift correction using spectral registration. *Magn Reson Med*. 2015;73:44-50.
 80. Pérez-Ruiz A, Julià-Sapé M, Mercadal G, Olier I, Majós C, Arús C. The INTERPRET decision-support system version 3.0 for evaluation of magnetic resonance spectroscopy data from human brain tumours and other abnormal brain masses. *BMC Bioinform*. 2010;11:581.
 81. Julia-Sape M, Lurgi M, Mier M, et al. Strategies for annotation and curation of translational databases: the eTUMOUR project. *Database*. 2012;2012:bas035.
 82. Vanhamme L, Sundin T, Hecke PV, Huffel SV. MR spectroscopy quantitation: A review of time-domain methods. *NMR Biomed*. 2001;14:233-246.
 83. Pouillet JB, Sima DM, van Huffel S. MRS signal quantitation: a review of time- and frequency-domain methods. *J Magn Reson*. 2008;195:134-144.
 84. Ratiney H, Sdika M, Coenradie Y, Cavassila S, Ormondt D, Graveron-Demilly D. Time-domain semi-parametric estimation based on a metabolite basis set. *NMR Biomed*. 2005;18:1-13.
 85. Maudsley AA, Domenig C, Govind V, et al. Mapping of brain metabolite distributions by volumetric proton MR spectroscopic imaging (MRSI). *Magn Reson Med*. 2009;61:548-559.
 86. Gal Y, Ghahramani Z. Dropout as a Bayesian approximation: representing model uncertainty in deep learning. Paper presented at: Proceedings of the 33rd International Conference on Machine Learning. vol. 48. New York, NY, USA; 2016: 1050-1059.
 87. Kendall A, Gal Y. What uncertainties do we need in Bayesian deep learning for computer vision? Paper presented at: 31st Conference on Neural Information Processing Systems (NIPS 2017); 2017; Long Beach, CA.
 88. Chawla NV, Bowyer KW, Hall LO, Kegelmeyer WP. SMOTE: synthetic minority over-sampling technique. *J Artif Intell Res*. 2002;16:321-357.
 89. Wilson M, Reynolds G, Kauppinen RA, Arvanitis TN, Peet AC. A constrained least-squares approach to the automated quantitation of in vivo ^1H magnetic resonance spectroscopy data: automated quantitation of In vivo ^1H MRS data. *Magn Reson Med*. 2011;65:1-12.
 90. Vicente J, Fuster-Garcia E, Tortajada S, et al. Accurate classification of childhood brain tumours by in vivo ^1H MRS - a multi-centre study. *Eur J Cancer*. 2013;49:658-667.
 91. Lin A, Andronesi O, Bogner W, et al. Minimum reporting standards for in vivo magnetic resonance spectroscopy (MRSin-MRS): experts' consensus recommendations. *NMR Biomed*. 2021;34:e4484. doi:10.1002/nbm.4484
 92. Olliverre N, Asad M, Yang G, Howe F, Slabaugh G. Pairwise mixture model for unmixing partial volume effect in multi-voxel MR spectroscopy of brain tumour patients. Paper presented at: Medical Imaging 2017: Computer-Aided Diagnosis. Orlando, FL, USA; 2017:449-461.
 93. Soffer S, Ben-Cohen A, Shimon O, Amitai MM, Greenspan H, Klang E. Convolutional neural networks for radiologic images: a radiologist's guide. *Radiology*. 2019;290:590-606.

94. Bhatt D, Patel C, Talsania H, et al. CNN variants for computer vision: history, architecture, application, challenges and future scope. *Electronics*. 2021;10:2470.
95. Alzubaidi L, Zhang J, Humaidi AJ, et al. Review of deep learning: concepts, CNN architectures, challenges, applications, future directions. *J Big Data*. 2021;8:53.
96. Jun L, Junyu C, Yucheng T, Ce W, Landman BA, Kevin ZS. Transforming medical imaging with transformers? A comparative review of key properties, current progresses, and future perspectives. *Med Image Anal*. 2023;85:102762.
97. Carlini N, Wagner D. Towards evaluating the robustness of neural networks. Paper presented at: 2017 IEEE Symposium on Security and Privacy (SP). San Jose, CA, USA; 2017:39-57.
98. Shlezinger N, Whang J, Eldar YC, Dimakis AG. Model-based deep learning. *Proc IEEE*. 2023;111:465-499.

How to cite this article: van de Sande DMJ, Merkofer JP, Amirrajab S, et al. A review of machine learning applications for the proton MR spectroscopy workflow. *Magn Reson Med*. 2023;90:1253-1270. doi: 10.1002/mrm.29793